Helicity-Preserving Optical Cavity Modes for Enhanced Sensing of Chiral Molecules

Joshua Feis,[1] Dominik Beutel,[2] Julian Köpfler,[1,3] Xavier Garcia-Santiago,[3,4] Carsten Rockstuhl,[2,3]
Martin Wegener ●,[1,3] and Ivan Fernandez-Corbaton ●[3]

[1]*Institute of Applied Physics, Karlsruhe Institute of Technology, 76128 Karlsruhe, Germany*
[2]*Institute of Theoretical Solid State Physics, Karlsruhe Institute of Technology, 76128 Karlsruhe, Germany*
[3]*Institute of Nanotechnology, Karlsruhe Institute of Technology, 76021 Karlsruhe, Germany*
[4]*JCMWave GmbH, 14050 Berlin, Germany*

Researchers routinely sense molecules by their infrared vibrational "fingerprint" absorption resonances. In addition, the dominant handedness of chiral molecules can be detected by circular dichroism (CD), the normalized difference between their optical response to incident left- and right- handed circularly polarized light. Here, we introduce a cavity composed of two parallel arrays of helicity-preserving silicon disks that allows one to enhance the CD signal by more than 2 orders of magnitude for a given molecule concentration and given thickness of the cell containing the molecules. The underlying principle is first-order diffraction into helicity-preserving modes with large transverse momentum and long lifetimes. In sharp contrast, in a conventional Fabry-Perot cavity, each reflection flips the handedness of light, leading to large intensity enhancements inside the cavity, yet to smaller CD signals than without the cavity.

DOI: 10.1103/PhysRevLett.124.033201

The interplay of molecules with nearby metallic or dielectric nanostructures allows for effectively enhancing light-molecule interaction. Examples are surface-enhanced Raman scattering [1–3], molecule infrared vibrational absorption resonances enhanced by plasmonic antennas [4], molecules in the near field of whispering-gallery-mode optical resonators [5], and largely enhanced molecular spontaneous emission rates in the vicinity of silver nanocubes [6]. Furthermore, frequency-selective optical metasurfaces can effectively integrate an otherwise necessarily external optical spectrometer [7].

However, all of the mentioned techniques are typically not able to sense the dominant handedness of chiral molecules. This aspect is important, though. For example, the majority of today's drugs use molecules of only one handedness (i.e., one enantiomer). Sometimes, the wrong molecule handedness has perturbing side effects. Therefore, enhancing the circular dichroism (CD) signal is highly desirable, especially if only small quantities of analyte with small concentrations of molecules are accessible. Early on, it was expected that the interaction of chiral nanostructures with chiral molecules would be helpful ([8], chapter 5, [9,10]). However, more recent work shows that the chirality of the nanostructure itself is rather unwanted [11–14], since it distorts the CD measurements, for example, by producing a nonzero signal even for racemic solutions or achiral molecules. The work in Ref. [14] also shows that the achiral nanostructure should be helicity preserving, such that the near field and the scattered far field have the same handedness as the incident light. Along these lines, systems for enhancing CD signals have been reported [13–18]. However, the spatial region of enhancement was restricted to only parts of the optical near field, which extended over a few hundreds of nanometers or less. Therefore, merely a small fraction of molecules in a microfluidic channel would experience this enhancement, hence reducing the total CD enhancement factor to near unity, that is, to no beneficial effect at all. This aspect severely limits the practicability of these previous approaches.

In this Letter, we design, describe, and characterize a cavity composed of two parallel dielectric metasurfaces. The cavity features approximately helicity-preserving modes with long lifetimes, leading to resonant CD enhancement factors exceeding one hundred, for cavity lengths of a few tens of micrometers. To achieve feedback, this cavity does not exploit the normal-incidence reflection off the metasurfaces. For an ordinary mirror, this reflection would convert left-handed into right-handed circularly polarized light and *vice versa*, destroying any positive effect of the cavity on the CD. The cavity rather exploits modes whose lifetime and helicity preservation are inherently large because their momentum is nearly parallel to the disk array plane. The long interaction times allow to selectively and resonantly enhance certain chiral molecular spectral resonances.

We proceed by showing that planar cavity modes with large transverse momentum feature long lifetimes and helicity preservation. The latter is a generic property that also occurs for light reflected at grazing incidence off a dielectric half-space. We then design a tunable cavity using two diffracting silicon disk arrays and numerically analyze its CD enhancement performance. Finally, we show that the

spatial regions of high enhancement inside the cavity are away from the near-field regions attached to the disks. To the best of our knowledge, this kind of cavity design has not been reported before.

A set of design requirements that lead to structures suitable for molecular CD enhancement has recently been formalized [14]: Achirality, helicity preservation, and strong light-matter interaction. The paradigmatic system for enhancing light-matter interaction is a cavity. An achiral cavity with helicity-preserving modes with long lifetimes would be a distinctly advantageous system for CD enhancement. Helicity-preserving resonances in achiral systems are a challenging requirement, though. Such resonances are, in principle, perfect mixes of the two helicities. The eigenmodes of systems with spatial inversion symmetries will also be eigenmodes of at least one of those inversion operations, and can hence be classified by their inversion eigenvalue $\tau = \pm 1$ ([19], page 181). For example, the electric and magnetic resonant modes in spheres are eigenstates of the parity operator, and the modes in planar waveguides are classified as TE or TM depending on their eigenvalue upon transformation by a mirror symmetry of the system. While the relevant inversion operator can be different in each system, the modes of achiral systems can always be written as the sum or subtraction of equal amplitude modes of well-defined helicity $\chi = \pm 1$ ([20], Sec. 2.4.2),

$$\sqrt{2}|\eta\,\tau\rangle = |\eta\chi = +1\rangle + \tau|\eta\chi = -1\rangle, \qquad (1)$$

where η is a composite index that completes the characterization of the mode [21]. Helicity preservation is hence not expected from isolated eigenmodes of systems with spatial inversion symmetry. However, helicity-preserving modes are achieved when a pair of $|\eta\,\tau = \pm 1\rangle$ modes becomes degenerate ([22], page 4). Upon degeneracy, any linear combination of the $\tau = \pm 1$ modes is also a modal solution, and the resonance preserves the polarization state of the excitation. This statement applies in particular to the pure helicity $\chi = \pm 1$ combinations,

$$\sqrt{2}|\eta\chi\rangle = |\eta\,\tau = +1\rangle + \chi|\eta\,\tau = -1\rangle. \qquad (2)$$

We now show that modes with large transverse momentum in planar cavities become helicity-preserving resonances. We start by arguing that degeneracy-induced helicity preservation is achieved quite generally in the reflection off planar systems in the limit of grazing incidence angle [23]. Let us consider a unit amplitude circularly polarized plane wave propagating in medium 1 and reflecting off a planar interface with medium 2. Both media are isotropic and homogeneous. We denote by β the angle of incidence measured with respect to the normal. It follows from Eqs. (1) and (2) that the reflected plane wave contains the two helicity components with coefficients

$$h_c = \frac{1}{2}(r_{\mathrm{TE}} + r_{\mathrm{TM}}), \qquad h_f = \frac{1}{2}(r_{\mathrm{TE}} - r_{\mathrm{TM}}), \quad (3)$$

for the preserved and flipped helicity component, respectively, where $r_{\mathrm{TE}}(r_{\mathrm{TM}})$ is the Fresnel reflection coefficient for the TE (TM) polarization, which depends on β and on the material parameters. It is readily seen from the expressions of the Fresnel reflection coefficients that, when $\beta \to \pi/2$, $r_{\mathrm{TE}} \to -1$ and $r_{\mathrm{TM}} \to -1$, independently of the material parameters. See Sec. I of Supplemental Material for a short derivation of this known phenomenon. Importantly, the same limiting behavior, $\lim_{\beta \to \pi/2} r_{\mathrm{TE}}(r_{\mathrm{TM}}) \to -1$, occurs in more general kinds of interfaces featuring (discrete) transverse translational symmetry, including anisotropic media and (diffracting) gratings ([24], chapter 2.3, [25]). We therefore see from Eq. (3) that the intensity of the flipped helicity component ($|h_f|^2$) tends to 0 as $\beta \to \pi/2$. This mechanism of helicity preservation as $\beta \to \pi/2$ can be seen on the one hand as the opposite of the complete helicity flipping for reflection when $\beta = 0$, and on the other hand as the reflection counterpart of the perfect helicity preservation for transmission at $\beta = 0$.

Let us now consider the modes of a slab waveguide. The effect discussed above suggests that, as $\beta \to \pi/2$, the TE and TM modes of the waveguide degenerate into helicity-preserving modes. That this is indeed the case can readily be seen from the expressions for the modal condition in a slab waveguide [[26], Eqs. (8.121) and (8.122)], which, in our notation, read as

$$2Lk\cos\beta + 2\Phi_{\mathrm{TE/TM}} = 2\pi l_{\mathrm{TE/TM}},$$

$$\Phi_{\mathrm{TE}} = -2\arctan\left(\sqrt{\frac{2\Sigma}{\cos^2\beta} - 1}\right),$$

$$\Phi_{\mathrm{TM}} = -2\arctan\left(\frac{1}{1 - 2\Sigma}\sqrt{\frac{2\Sigma}{\cos^2\beta} - 1}\right),$$

$$(4)$$

where L is the thickness of the slab, k is the wavenumber inside the slab, $l_{\mathrm{TE}}(l_{\mathrm{TM}})$ is an integer, and $2\Sigma = 1 - (n_2/n_1)^2$, where $n_1(n_2)$ is the refractive index of the slab (exterior region). As before, when $\beta \to \pi/2$, $\Phi_{\mathrm{TE}} \to \pi$ and $\Phi_{\mathrm{TM}} \to \pi$, and the TE and TM modes become degenerate. Therefore, modes of large transverse momentum become helicity-preserving resonances. This physical insight can be used for designing a system for enhanced CD measurements.

Let us imagine that we place two planar substrates facing each other and leave a gap between them forming a cavity, which plays the role of the slab. The gap is to be filled with the solution of chiral molecules. We then need a means for exciting modes with large β, and then measuring the outgoing power. This is not trivial because large β implies a large momentum component in a direction transverse to
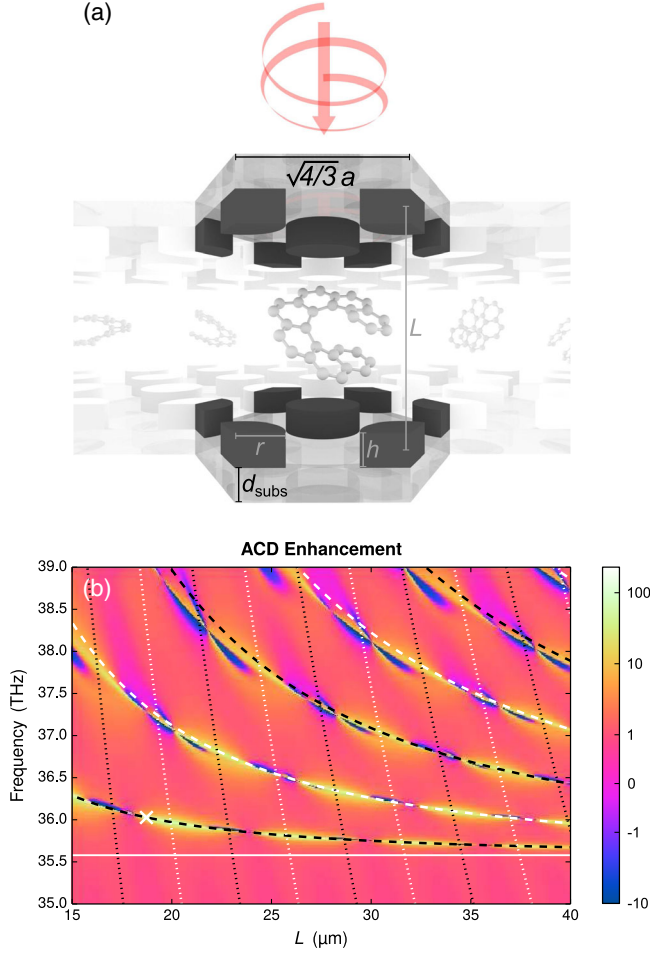
(a)

(b)

ACD Enhancement

FIG. 1.   (a) Sketch of the cavity and illumination (not to scale). The dimensions are, in micrometers, $a = 5.76$, $h = 1.32$, $r = 1.92$, and $d_{\text{subs}} = 2.0$. The disks are made out of silicon and the dielectric substrates have $\epsilon_{\text{subs}} = 2.14$. (b) Absorbance CD enhancement achieved by the system under perpendicular illumination as a function of frequency and cavity length (L). The scale is a symmetric logarithmic scale (see the text). The dashed (dotted) lines are approximated modal conditions for modes composed of the first (zeroth) array diffraction orders. The solid horizontal line marks the onset of diffraction in an $\epsilon_r = 2.14$ medium.

the cavity walls, which, together with the refractive index of the solvent, prevent such modes to couple directly to electromagnetic waves propagating in air, whose momentum is insufficient. One possible solution is to add diffracting arrays for providing the necessary momentum matching for both excitation and measurement along the normal $\pm z$ directions. The structure that we propose is a cavity formed by two identical planar arrays of cylinders placed opposite each other at a distance L. The cylinders are arranged in the form of hexagonal lattices and are supported by finite-thickness substrates that seal the chamber. Figure 1(a) shows a sketch of the cavity. The intended functionality is that, upon circularly polarized perpendicular illumination from the top array, a diffraction

order excites an approximately helicity-preserving resonant mode in the cavity. The light then interacts with the molecules for some time determined by the lifetime of the resonance. Finally, again thanks to diffraction off the arrays, the light can couple out of the cavity along the $\pm z$ directions, where detectors are placed.

While the modes in a cavity like the one that we propose are more complex than in a slab waveguide, they can still be classified as TE or TM. We can hence expect that, because the specular reflection from a single array behaves similarly to the case of a planar interface, the cavity modes with large transverse momentum will become helicity-preserving resonances. In Supplemental Material we analyze the zeroth-order reflection coefficient for a single diffracting array of silicon disks embedded in an $\epsilon_r = 2.14$ medium as a function of frequency, and incidence angle β. Figure S4(a) shows the helicity change measure $|h_f|^2/(|h_c|^2 + |h_f|^2)$ for the zeroth-order (specular) reflection. Figure S4(b) shows the real part of h_c. The results meet the expectation: As $\beta \rightarrow \pi/2, h_c \rightarrow -1$ and $|h_f|^2 \rightarrow 0$. Two distinct lines where the convergence is much slower can be observed. They correspond to modes of the single array. Importantly, we note that a mode with $\beta \rightarrow \pi/2$ automatically has a long lifetime because when $|h_c| \rightarrow 1$, the coupling to the channels through which the energy can leave the mode tends to 0 due to energy conservation. This implication is quantitatively verified in Fig. S4(c), which shows that the average number of internal reflections before the energy leaves the mode grows as $\beta \rightarrow \pi/2$. That this happens in a diffracting array is quite remarkable.

We now investigate the CD enhancement performance of the design. We use the following definition of absorbance CD (ACD),

$$\text{ACD} = \frac{P_+ - P_-}{2P_0}, \tag{5}$$

where P_+ and P_- are the outgoing powers for left-handed ("+") and right-handed ("-") circularly polarized incident light, for identical incident powers equal to P_0. The outgoing power includes both transmitted and reflected fields. The ACD measures the differential absorption of the molecules relative to the incident power. We also consider the transmittance CD (TCD), defined as $(P_+^{\text{fwd}} - P_-^{\text{fwd}})/(P_+^{\text{fwd}} + P_-^{\text{fwd}})$, where only the transmitted powers $P_\pm^{\text{fwd}}$ are detected. The ACD (TCD) enhancement factor is defined by the ACD (TCD) signal with the arrays divided by that without the arrays.

The chiral solution in the cavity is modeled by the constitutive relations

$$\mathbf{D} = \epsilon_0\epsilon_r\mathbf{E} + i\frac{\kappa}{c_0}\mathbf{H} \quad \text{and} \quad \mathbf{B} = \mu_0\mu_r\mathbf{H} - i\frac{\kappa}{c_0}\mathbf{E}, \tag{6}$$

where $\epsilon_r = 2.14 + i10^{-4}$, $\mu_r = 1 + i10^{-4}$, and $\kappa = i10^{-4}$. The dielectric permittivity of the substrates is assumed to be

equal to $\epsilon_{\text{subs}} = 2.14$. These material parameters are realistic choices for substrates and many solvents commonly used in infrared measurements of chiral molecules [27]. The cylinders are made out of silicon with $\epsilon_{\text{cyl}} = 11.9$ and $\mu_{\text{cyl}} = 1$. Regarding the numerical analysis, we refer the reader to Sec. V of Supplemental Material for details. Figure 1(b) shows the ACD enhancement in a symmetric logarithmic scale [28] as a function of the array-to-array distance L and the illumination frequency f. The ACD enhancement is larger than thirtyfold in several areas along a set of curved lines. The enhancement is higher around the lowest lying line where it reaches a maximum value of 126 at $(L, f) = (18.73\ \mu\text{m}, 36.03\ \text{THz})$. This point is marked with a white cross. The onset of diffraction, where $\beta = \pi/2$, occurs at $f = 35.58\ \text{THz}$ and is marked by the white continuous line. The curved dashed lines are computed using

$$L\sqrt{1 - \left(\frac{\lambda}{a}\right)^2} = \frac{\lambda}{2}(l_1 - 1), \tag{7}$$

for integer $l_1 - 1 \in \{1, \ldots, 6\}$, where λ is the wavelength in an $\epsilon_r = 2.14$ medium, and $\sqrt{(4/3)}a$ is the center-to-center distance between the disks. Lower values of $l_1 - 1$ correspond to lines closer to the diffraction limit. We show in Sec. II of the Supplemental Material that Eq. (7) is the approximated modal condition for the first six frequency degenerate diffraction orders from the hexagonal lattice upon normal incidence. The -1 on the right-hand side of Eq. (7) arises from the phase of π acquired upon reflection at large incidence angles. We can also observe in Fig. 1(b) that the enhancement has some dips along the lines. These are due to coupling between the first diffraction orders and the zeroth diffraction orders, whose modal equation is [see Eq. (S6)]

$$L = \frac{\lambda}{2}l_0. \tag{8}$$

The dotted lines in Fig. 1(b) correspond to Eq. (8) for integer $l_0 \in \{6, \ldots, 15\}$. The enhancement dips do not occur at every crossing of the lines determined by Eqs. (7) and (8), but rather in an alternating fashion. As shown in [29], Sec. 2.3c, two different kinds of modes can couple when the phase that they accumulate in a half round-trip is an integer multiple of 2π. We show in Sec. II that they can couple when $l_1 - l_0$ is even or, equivalently, when $(l_1 - 1) - l_0$ is odd. In Fig. 1(b), the crossings of dashed and dotted lines of the same color mark points where the two kinds of modes can couple. At these points, the grazing incidence angle properties of the first-order modes cease to exist in the resulting mixed modes, and the enhancement disappears. The first-order modes are unperturbed in the crossings of dashed and dotted lines of different color. The maximum enhancement occurs at $L = 18.73\ \mu\text{m}$ in the lowest lying line [30], which corresponds to $\beta \approx 81$ degrees [Eq. (S10)].
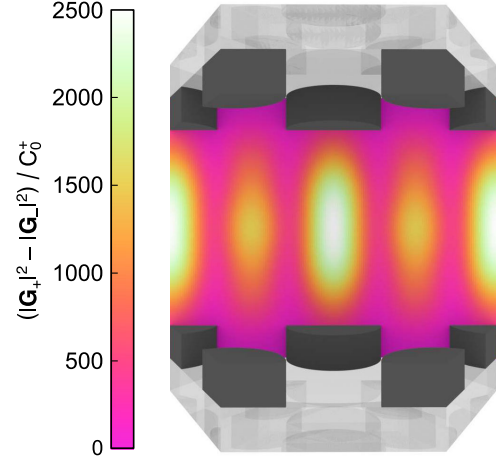

FIG. 2. Spatial intensity maps of the helicity density enhancement inside the cavity for $(L, f) = (18.73\ \mu\text{m}, 36.03\ \text{THz})$.

It should be noted that the first six diffraction orders can propagate in the cavity and in the substrates, but become evanescent in vacuum [31]. The system is hence non-diffracting for external illumination and measurement: All the information about the internal light-matter interaction available outside the system is contained in the zeroth transmission and reflection orders.

In many CD measurement setups, only the transmitted power is detected. Figure S1 in Supplemental Material shows the transmittance CD enhancement, where features and enhancement values very similar to those seen in Fig. 1(b) can be observed. While in a few regions the TCD enhancement can be partly due to a sharp decrease in transmittance, Fig. S2 shows that this is not the general case, and that the averaged forward transmitted power $(P_+^{\text{fwd}} + P_-^{\text{fwd}})/2$ is relatively large for many high enhancement regions. We also note that the incoupling causes some helicity non-preservation [32].

An important property that distinguishes the cavity from previous proposals is that the regions of high enhancement are not just the near fields around the cylinders. We now study the local enhancement as a function of position inside the cavity. We make use of the pointwise square norms of the two helicity components of the field $|\mathbf{G}_+(\mathbf{r})|^2$, and $|\mathbf{G}_-(\mathbf{r})|^2$, where $\sqrt{2}\mathbf{G}_\pm(\mathbf{r}) = \mathbf{E}(\mathbf{r}) \pm iZ\mathbf{H}(\mathbf{r})$, with Z being the medium impedance, are Riemann-Silberstein-like vectors [33]. The ratio between the difference $|\mathbf{G}_+(\mathbf{r})|^2 - |\mathbf{G}_-(\mathbf{r})|^2 = \gamma(\mathbf{r})$ for the cases with $[\gamma_c(\mathbf{r})]$ and without $[\gamma_0(\mathbf{r})]$ the structure is the pointwise enhancement of the helicity density due to the cavity, which is identical to the ratio between the optical chirality density [34] for those same cases. For an achiral system with properly chosen illumination the volume integral of $\gamma_c(\mathbf{r})/\gamma_0(\mathbf{r})$ is a good proxy for the CD enhancement [14]. We assume that the cavity is filled with a medium characterized by $\epsilon_r = 2.14$, $\mu_r = 1$, and $\kappa = 0$. The structure is illuminated with a left-handed polarized plane wave under perpendicular incidence. Its

helicity intensities are $|\mathbf{G}_+^0(\mathbf{r})|^2 = C_+^0 \neq 0$ and $|\mathbf{G}_-^0(\mathbf{r})|^2 = 0$. Figure 2 shows the spatial maps of $\gamma_c(\mathbf{r})/\gamma_0(\mathbf{r}) = \gamma_c(\mathbf{r})/C_+^0$ for $(L, f) = (18.73 \mu\text{m}, 36.03 \text{THz})$. We observe that the helicity density enhancement is large in electromagnetically large volumes, and that it increases when going away from the cylinders towards the center of the cavity, well outside the near-field regions around the cylinders.

Finally, in Sec. IV of Supplemental Material [35] we perform a quantitative analysis of the effects of violating the achirality requirement in our proposed cavity. We show that a nonzero ACD signal can be measured from an achiral analyte when the mirror symmetries of the cavity are broken due to a relative transverse displacement between the two arrays. This aspect needs to be considered in the manufacturing of such CD-enhancing cavities.

In conclusion, we have presented a planar cavity that enhances the circular dichroism signal of chiral molecules by 2 orders of magnitude. The design exploits helicity-preserving cavity modes with long lifetimes that are mediated by the TE/TM reflection degeneracy in the limit of grazing incidence angle.

[1] D. L. Jeanmaire and R. P. V. Duyne, J. Electroanal. Chem. **84**, 1 (1977).

[2] K. Kneipp, Y. Wang, H. Kneipp, L. T. Perelman, I. Itzkan, R. R. Dasari, and M. S. Feld, Phys. Rev. Lett. **78**, 1667 (1997).

[3] M. I. Stockman, Electromagnetic theory of SERS, in *Surface-Enhanced Raman Scattering: Physics and Applications*, edited by K. Kneipp, M. Moskovits, and H. Kneipp (Springer Berlin Heidelberg, Berlin, Heidelberg, 2006), pp. 47–65.

[4] R. Adato, A. A. Yanik, J. J. Amsden, D. L. Kaplan, F. G. Omenetto, M. K. Hong, S. Erramilli, and H. Altug, Proc. Natl. Acad. Sci. U.S.A. **106**, 19227 (2009).

[5] A. M. Armani, R. P. Kulkarni, S. E. Fraser, R. C. Flagan, and K. J. Vahala, Science **317**, 783 (2007).

[6] G. M. Akselrod, C. Argyropoulos, T. B. Hoang, C. Cirac, C. Fang, J. Huang, D. R. Smith, and M. H. Mikkelsen, Nat. Photonics **8**, 835 (2014).

[7] A. Tittl, A. Leitis, M. Liu, F. Yesilkoy, D.-Y. Choi, D. N. Neshev, Y. S. Kivshar, and H. Altug, Science **360**, 1105 (2018).

[8] M. Schäferling, Springer Ser. Opt. Sci. **205**, 159 (2016).

[9] M. Hentschel, M. Schäferling, T. Weiss, N. Liu, and H. Giessen, Nano Lett. **12**, 2542 (2012).

[10] V. K. Valev, J. J. Baumberg, C. Sibilia, and T. Verbiest, Adv. Mater. **25**, 2517 (2013).

[11] T. Wu, J. Ren, R. Wang, and X. Zhang, J. Phys. Chem. C **118**, 20529 (2014).

[12] M. L. Nesterov, X. Yin, M. Schaferling, H. Giessen, and T. Weiss, ACS Photonics **3**, 578 (2016).

[13] E. Mohammadi, K. L. Tsakmakidis, A. N. Askarpour, P. Dehkhoda, A. Tavakoli, and H. Altug, ACS Photonics **5**, 2669 (2018).

[14] F. Graf, J. Feis, X. Garcia-Santiago, M. Wegener, C. Rockstuhl, and I. Fernandez-Corbaton, ACS Photonics **6**, 482 (2019).

[15] S. J. Yoo and Q.-H. Park, Phys. Rev. Lett. **114**, 203003 (2015).

[16] J. García-Guirado, M. Svedendahl, J. Puigdollers, and R. Quidant, Nano Lett. **18**, 6279 (2018).

[17] A. Vázquez-Guardado and D. Chanda, Phys. Rev. Lett. **120**, 137601 (2018).

[18] M. L. Solomon, J. Hu, M. Lawrence, A. García-Etxarri, and J. A. Dionne, ACS Photonics **6**, 43 (2019).

[19] E. P. Wigner, *Group Theory and Its Application to the Quantum Mechanics of Atomic Spectra* (Academic Press, New York, 1959).

[20] I. Fernandez-Corbaton, Helicity and duality symmetry in light matter interactions: Theory and applications, Ph.D. thesis, Macquarie University, 2014, arXiv:1407.4432.

[21] For example, for spherical waves η is composed by the frequency, total angular momentum, and angular momentum along a chosen axis.

[22] I. Fernandez-Corbaton, X. Zambrana-Puyalto, N. Tischler, X. Vidal, M. L. Juan, and G. Molina-Terriza, Phys. Rev. Lett. **111**, 060401 (2013).

[23] General degeneracy, independent of anything else, is achieved if the system has electromagnetic duality symmetry. This is easily seen from the action of the generator of duality, the helicity operator Λ, on the τ eigenstates: $\Lambda\sqrt{2}|\eta\tau\rangle = \sqrt{2}\Lambda(|\eta+\rangle + \tau|\eta-\rangle) = \sqrt{2}(|\eta+\rangle - \tau|\eta-\rangle) = \sqrt{2}|\eta-\tau\rangle$. Since the $\tau = \pm 1$ modes transform into each other by the action of the generator of a symmetry of the system, they must be degenerate. Systems whose materials have all the same impedance, $Z_i = \sqrt{\mu_i/\epsilon_i} = Z$ for all i, are dual symmetric [22]. Dual systems are challenging to obtain, specially for near infrared and higher frequencies. As seen in Eq. (S1), $r_{\text{TE}} = r_{\text{TM}}$ is achieved for all β if and only if $Z_1 = Z_2$ [22].

[24] J. Lekner, *Theory of Reflection: Reflection and Transmission of Electromagnetic, Particle and Acoustic Waves* (Springer, New York, 2016), Vol. 87.

[25] J. Nakayama, IEICE T. Electron. **E94.C**, 2 (2011).

[26] J. D. Jackson, *Classical Electrodynamics* (Wiley, New York, 1998).

[27] L. D. S. Yadav, *Organic Spectroscopy* (Springer Science & Business Media, Heidelberg, 2013).

[28] The logarithm of the quantity for positive values larger than 1, the negative logarithm of the absolute value of the quantity for negative values smaller than −1, and a linear interval from −1 to 1.

[29] C. J. Chang-Hasnain and W. Yang, Adv. Opt. Photonics **4**, 379 (2012).

[30] The increasingly finer enhancement linewidths as $\beta \to \pi/2$ makes it increasingly more difficult to reliably evaluate the enhancements for angles very close to 90 degrees.

[31] In vacuum, the diffraction-free region extends up to ≈ 52 THz.

[32] Our numerical calculations show that the transmission from perpendicular incidence to the first diffraction order features a helicity preservation degree of $\approx 82\%$ between 35.6 and 38.5 THz.

[33] I. Bialynicki-Birula and Z. Bialynicka-Birula, J. Phys. A **46**, 053001 (2013).

[34] Y. Tang and A. E. Cohen, Phys. Rev. Lett. **104**, 163901 (2010).

[35] See Supplemental Material at http://link.aps.org/supplemental/10.1103/PhysRevLett.124.033201, which includes Refs. [36–40].

[36] N. Stefanou, V. Yannopapas, and A. Modinos, Comput. Phys. Commun. **132**, 189 (2000).

[37] M. I. Mishchenko, N. T. Zakharova, N. G. Khlebtsov, G. Videen, and T. Wriedt, J. Quant. Spectrosc. Radiat. Transfer **178**, 276 (2016).

[38] M. Fruhnert, I. Fernandez-Corbaton, V. Yannopapas, and C. Rockstuhl, Beilstein J. Nanotechnol. **8**, 614 (2017).

[39] G. Demésy, J.-C. Auger, and B. Stout, J. Opt. Soc. Am. A **35**, 1401 (2018).

[40] X. G. Santiago, M. Hammerschmidt, S. Burger, C. Rockstuhl, I. Fernandez-Corbaton, and L. Zschiedrich, Phys. Rev. B **99**, 045406 (2019).